A Physical Model of Contact Resistance in Ti-Contacted Graphene-Based Field Effect Transistors

Bin Wang, Mohammad Wasil Malik, Yiyi Yan, Valeriya Kilchytska, Yun Zeng, Denis Flandre, *Senior Member, IEEE*, and Jean-Pierre Raskin, *Fellow, IEEE*

***Abstract*— The effect of device fabrication processing conditions is often overlooked in the evaluation of the contact resistance in metal–graphene contact. In this work, we investigate the Ti–graphene contact resistance theoretically and experimentally. A compact model has been proposed to reveal and evaluate the role of different factors in controlling the value of contact resistance. A layer of oxidized Ti or polymer residues at the Ti–graphene interface has been considered to explain the reduced carrier transmission probability through the interface. Experimental results report a low contact resistance as small as 271.45 Ω ·μm and our model agrees with the measured values. The proposed model explains the large variation of the contact resistance reported in the literature up to date and help to improve metal–graphene contact for future applications.**

***Index Terms*— Contact resistance, graphene, interfacial layer, model.**

I. Introduction

GRAPHENE is considered to be a promising material for future high-speed and high-frequency transistors due to its superior electrical properties [1], [2]. However, the metal–graphene contact resistance (R_c) becomes the key bottleneck limiting the device performance when the device dimension is scaled down. Ti is widely used as an electrode in carbon-based devices due to its excellent adhesion property. It has been theorized to form chemical contact with graphene together with other metals like Ni, Cr, Pd, etc., [3], [4]. Differing from physical contact, chemical contact is expected to achieve low contact resistance due to the strong interaction between chemisorbed metals and graphene. However, the up to date reported measurement results of R_c are inconsistent, varying from 10^2–10^4 Ω·μm [5]–[9]. A systematic model is required to reveal the factors in controlling the value of R_c. Xia *et al.* [10] proposed a model in which R_c is dominated by two cascaded carrier transport processes: initial carrier injection from metal to graphene followed by the transport to the channel, with probabilities T_{mg} and T_{gg}, respectively. However, the mechanism of T_{mg} is ambiguous, and it has been theoretically investigated that no tunneling barrier exists at ideal Pd or Ti/graphene interfaces [11]. Chaves *et al.* [12] proposed a model dividing the contact resistance into two parts R_{mg} and R_{gg}, where R_{mg} reflects the resistance of the metal–graphene interface and R_{gg} is the resistance due to the potential step of the junction formed between the graphene under metal and channel caused by the different doping level. However, both models overlooked the effect of processing conditions of the contact. In the general graphene device fabrication process, resist residues remain on the surface of graphene even after additional cleaning treatments such as UV–Ozone [13], annealing [14], and oxygen plasma [15]. Ti has been found to easily react with the residues to form oxidized islands on the graphene. Furthermore, the residue oxygen in the evaporation chamber enables the *in situ* oxidation of Ti [16]. Based on X-ray photoelectron spectroscopy (XPS) measurements, Freedy *et al.* [17] pointed out that the Ti oxide component is dependent on the base pressure of the chamber and the deposition rate. At a pressure of 1×10^{-7} Torr and deposition rate from 0.1 to 1 nm/s, 10% to 25% of Ti oxide has been measured in 5 nm thick Ti deposited on graphene capped by Au layer. Politou *et al.* [18] observed an oxide layer at Ti–graphene interface using transmission electron microscopy (TEM) and energy dispersive spectroscopy (EDS) characterizations. Furthermore, the polymer residues are inevitable in the fabrication process and may still exist at the Ti–graphene interface. The interfacial layer between Ti and graphene may prevent orbital hybridization and lower the carrier transmission probability, ultimately increasing the contact resistance. Therefore, the interfacial layer at Ti–graphene interface should be taken into account for the contact resistance modeling.

In this article, we consider an ultrathin uniform interfacial layer between metallic Ti and graphene. The carrier transmission probability through Ti/IL/graphene interfaces has been

Manuscript received September 13, 2020; revised November 23, 2020; accepted December 16, 2020. Date of publication January 8, 2021; date of current version January 22, 2021. This work was supported by the China Scholarship Council. The review of this article was arranged by Editor F. Schwierz. *(Corresponding author: Bin Wang.)*

Bin Wang is with the School of Physics and Electronics, Hunan University, Changsha 410082, China, and also with the Institute of Information and Communication Technologies, Electronics and Applied Mathematics (ICTEAM), Université catholique de Louvain, 1348 Louvain-la-Neuve, Belgium (e-mail: wangbin_qisui@hnu.edu.cn).

Mohammad Wasil Malik, Yiyi Yan, Valeriya Kilchytska, Denis Flandre, and Jean-Pierre Raskin are with the ICTEAM Institute, Université catholique de Louvain, 1348 Louvain-la-Neuve, Belgium (e-mail: mohammad.malik@uclouvain.be; yiyi.yan@uclouvain.be; valeriya.kilchytska@uclouvain.be; denis.flandre@uclouvain.be; jean-pierre.raskin@uclouvain.be).

Yun Zeng is with the School of Physics and Electronics, Hunan University, Changsha 410082, China (e-mail: yunzeng@hnu.edu.cn).

Color versions of one or more figures in this article are available at https://doi.org/10.1109/TED.2020.3046166.

Digital Object Identifier 10.1109/TED.2020.3046166

0018-9383 © 2021 IEEE. Personal use is permitted, but republication/redistribution requires IEEE permission.
See https://www.ieee.org/publications/rights/index.html for more information.

Authorized licensed use limited to: Univ Catholique de Louvain/UCL. Downloaded on February 22,2021 at 15:48:31 UTC from IEEE Xplore. Restrictions apply.

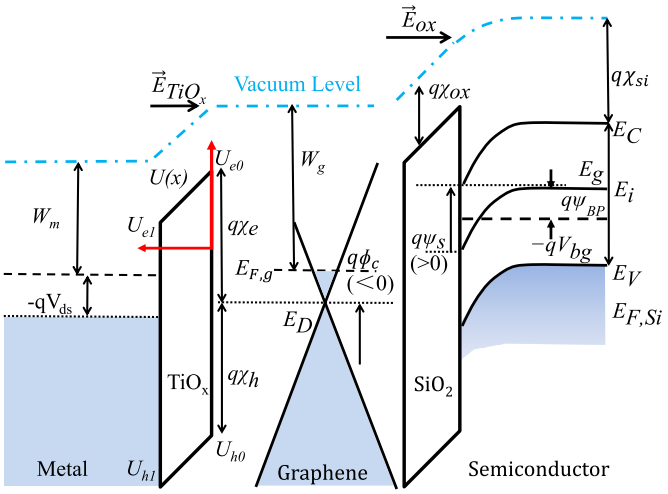


Fig. 1. Band diagram of the Ti/TiO_x/graphene/SiO_2/Si heterostructure. $U(x)$ is the potential profile in the oxidized Ti layer, U_{e0}, U_{e1}, and U_{h0}, U_{h1} are the band edges of the electrons and holes, respectively.

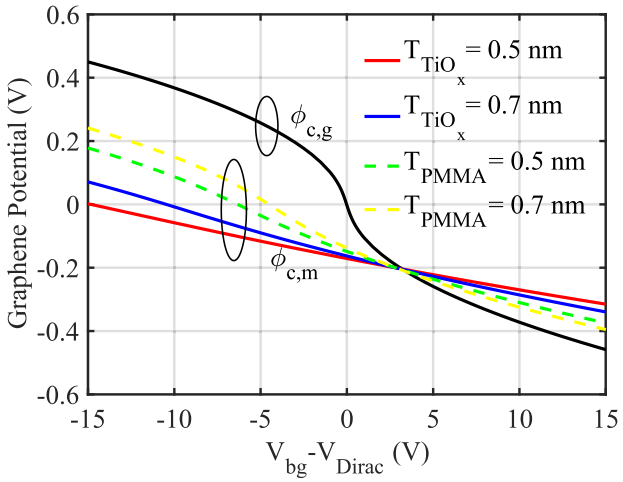


Fig. 2. Calculated graphene potential $\phi_{c,g}$ and $\phi_{c,m}$ as a function of gate bias for different T_{TiOx} and T_{PMMA}.

modeled. Combining the model of the transmission probability through the potential step, a compact model for the contact resistance is derived.

II. Electrostatics

Oxidized Ti as the interfacial layer is first utilized to illustrate our model. We consider three terminal graphene field effect transistors (GFETs) with back gate bias (V_{bg}) that the contact resistance at the drain side and source side is equivalent. The band diagram of the Ti/TiO_x/graphene/oxide/semiconductor heterostructure at the drain side is shown in Fig. 1. The conditions for energy conservation and charge neutrality are given in the following equations:

$$W_g - W_m + q\phi_{c,m} - qV_{ds} + qE_{TiO_x}T_{TiO_x} = 0 \quad (1)$$

$$-q(V_{bg} - V_{ds}) + q\psi_{Bp} - q\psi_s + \frac{1}{2}E_g + q\chi_{Si} - qE_{ox}T_{ox} - qW_g - q\phi_{c,m} = 0 \quad (2)$$

$$Q_{\text{net}} + Q_m + Q_s + Q_f = 0. \quad (3)$$

In (1), W_m (4.3 eV) and W_g (4.5 eV) are workfunctions of pure Ti and graphene, respectively. $\phi_{c,m}$ is the graphene potential under metal corresponding to the difference between the Fermi level and Dirac energies. V_{ds} is the drain–source bias. T_{TiO_x} is the thickness of the oxidized Ti due to the processing and E_{TiO_x} is the built-in electric field in the oxidized Ti. In (2), $\psi_{Bp} = k_B T \ln(N_A/n_i)$ with N_A the acceptor doping concentration and n_i the intrinsic concentration of the substrate. ψ_s is the surface potential, χ_{Si} is the silicon electron affinity, E_g is the silicon bandgap energy, E_{ox} the electric field in silicon oxide and T_{ox} is the thickness of the oxide (20 nm in this work). In (3), Q_{net} is the overall net mobile charge density given by Champlain [19]

$$Q_{\text{net}} = q(p-n) = \frac{2q(k_BT)^2}{\pi(\hbar v_F)^2}\left[\mathcal{F}_1\left(\frac{\phi_{c,m}}{k_BT}\right) - \mathcal{F}_1\left(-\frac{\phi_{c,m}}{k_BT}\right)\right]. \quad (4)$$

Here, p and n are the free carrier densities of holes and electrons, $\mathcal{F}_1$ is the first-order Fermi integral. k_B and T are the Boltzman constant and temperature, respectively. $\hbar$ is the reduced Plank's constant and $v_F \approx 1 \times 10^6$ m/s is the Fermi velocity. $Q_m = -\varepsilon_0\varepsilon_{TiO_x}E_{TiO_x}$ describes the charge per unit area induced in the metal, where ε_{TiO_x} is the relative permittivity of TiO_x and has been estimated to be 6.9 eV [16]. Q_f is the fixed charge density representing any fixed charges within graphene sheet [20]. Q_s is the surface potential given by Sze and Ng [21] in (5), with ε_{Si} the permittivity of silicon substrate, $L_D = \sqrt{\frac{2k_BT\varepsilon_{Si}}{q^2p_{p0}}}$ the Debye length for holes and $F(u)$ is given in (6). n_{p0} and p_{p0} are the equilibrium concentrations in the p-type substrate for electrons and holes, respectively

$$Q_s = -\text{sign}(\psi_s)\frac{2\varepsilon_s k_B T}{qL_D}F\left(\frac{\psi_s}{\phi_T}\right) \quad (5)$$

$$F(u) \triangleq \sqrt{(e^{-u}+u+1) + \frac{n_{p0}}{p_{p0}}(e^u - u - 1)}. \quad (6)$$

Based on the equations above, $\phi_{c,m}$ is computed as a function of gate bias and the thickness of TiO_x. The graphene potential assuming a layer of polymer residues has also been obtained with the relative permittivity of polymer $\varepsilon_{PMMA} = 3$. The potential of graphene in the channel $\phi_{c,g}$ can be obtained in a similar way by simply setting $Q_m = 0$ in (3). Fig. 2 shows the gate dependence of $\phi_{c,m}$ and $\phi_{c,g}$. We assume Q_f is the same for the computation for both $\phi_{c,m}$ and $\phi_{c,g}$. In calculating $\phi_{c,g}$, two different thickness of TiO_x (T_{TiO_x} = 0.5 and 0.7 nm) are considered. The n-doping effect induced by Ti has been observed, which is consistent with previous studies. The different potential between the graphene under metal and channel leads to the formation of potential step with effective length (λ) at contact edge.

III. Calculation of Contact Resistance

The carrier transport processes at Ti–TiO_x–graphene junction are presented in Fig. 3, with transmission probabilities T_{mg} and T_{gg}. Graphene under the metal has limited conduction modes. According to Landauer approach, contact resistance (R_c) is determined by T_{mg}, T_{gg} and the lowest conduction modes of graphene under the metal or in the channel. The contact resistance can be obtained by $R_c = \pi\hbar/2q^2T_{\text{total}}M$, where

Authorized licensed use limited to: Univ Catholique de Louvain/UCL. Downloaded on February 22,2021 at 15:48:31 UTC from IEEE Xplore. Restrictions apply.

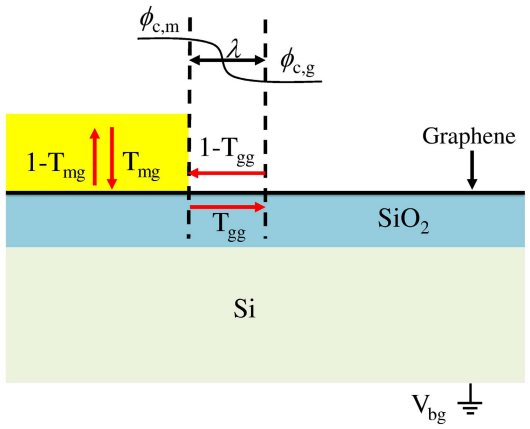


Fig. 3. Schematic view of the carrier transport processes at the Ti/graphene junction, with transmission probability T_{mg} and T_{gg}.

$T_{\text{total}} = T_{mg}T_{gg}/(1-(1-T_{mg})(1-T_{gg}))$ [22] the total carrier transmission probability, $M = \min(|\phi_{c,g}|, |\phi_{c,m}|)Wq/\pi\hbar v_F$ is the conduction modes, with graphene channel width W.

The probability of carrier transmission through the potential step (T_{gg}) with effective length (λ) is given by Cayssol *et al.* [23]

$$T_{gg} = 1 - \frac{\sinh(\pi\lambda\kappa^{+-})\sinh(\pi\lambda\kappa^{-+})}{\sinh(\pi\lambda\kappa^{--})\sinh(\pi\lambda\kappa^{++})} \tag{7}$$

where $\kappa^{ab} = q(\phi_{c,g}-\phi_{c,m})/\hbar v F + ak_x^g + bk_x^m$, with $a, b = \pm 1$. The relationship between the longitudinal momentum (k_x) and the transverse momentum (k_y) can be expressed by

$$k_x^i = \text{sgn}(\phi_{c,i})\sqrt{(q\phi_{c,i}/\hbar v F)^2 - k_y^2}, \quad i = m, g. \tag{8}$$

The density of states (DOS) broadening effect should also be considered for the modeling of the contact resistance. It has been theoretically investigated that the coupling strength between Ti and graphene is strong. However, the presence of the interfacial layer at Ti/graphene interface could inhibit the orbital hybridization and weakens the coupling, thus preserving the band structure of the graphene under metal. Therefore, the broadening of graphene in the channel is assumed to be inhomogeneous. We use Gaussian function $G(x,t) = \exp(-x^2/t^2)/(t\pi^{1/2})$ to model the broadening effect for graphene under metal and in the channel. R_c can be ultimately expressed as

$$R_c^{-1} = \frac{q^2}{\pi^2\hbar}\int_{-\infty}^{\infty} dE_1 G(qE_1 - q\phi_m, t_g) \times \int_{-\infty}^{\infty} dE_2 G(qE_2 - q\phi_g, t_m)\int_{-k_F}^{k_F} T_{\text{total}} dk_y \tag{9}$$

where $t_g = \hbar v_F(\sqrt{2\pi n_0})$ with n_0 the minimum carrier concentration in the graphene channel, t_m is the broadening energy of graphene under the metal, $k_F = \min|\phi_{c,g}, \phi_{c,m}|q/\hbar v_F$ is the Fermi momentum.

The carrier transmission T_{mg} through Ti–TiO_x–graphene interfaces is dependent on the tunneling mechanism and has been modeled based on quantum-mechanical tunneling theory. Taking the random disorder potential of the graphene under the metal into account, different tunneling mechanisms occur due to the change of the barrier shape at the Ti/TiOx/graphene interface. Electron tunneling and hole tunneling dominate the current when $E_1 < 0$ and $E_1 > 0$, respectively. Using the Wentzel– Kramers–Brillouin approximation (WKB), the tunneling probability T_{mg} of the electrons and holes with Fermi energy can be expressed as [21] (10), shown at the bottom of the page, where $\Delta_{\text{TiO}_x} = E_{\text{TiO}_x}T_{\text{TiO}_x}$, T_{TiO_x} is the thickness of the oxidized Ti layer. The band edges qU_{e0}, qU_{e1}, and qU_{h0}, qU_{h1} are given by

$$\begin{aligned} U_{e0} &= \chi_e + qE_1 \\ U_{e1} &= \chi_e + qE_1 - q|\Delta_{\text{TiO}_x}| \\ U_{h0} &= \chi_h - qE_1 \\ U_{h1} &= \chi_h - qE_1 - q|\Delta_{\text{TiO}_x} \end{aligned} \tag{11}$$

$\chi_e = W_m - \chi_{\text{TiO}_x}$ is the barrier height of undoped graphene. Given that the workfunction (W_m) of Ti is 4.3 eV and (χ_{TiO_x}) is the electron affinity of the oxidized Ti. We assume $\chi_e = \chi_h$ in our model. m_e and m_h are the effective mass of TiO_x.

According to our model, the contact resistance is dependent on several parameters. The value and definition of the parameters that we used to calculate the contact resistance is listed in Table I.

Figs. 4 and 5 show the calculated contact resistance as a function of gate bias for different values of t_m and λ, respectively. Two peaks are observed when the broadening energy $t_m < 0.3$ eV, one corresponding to the minimum DOS of graphene in the channel ($\phi_{c,g} = 0$) and the other locates in the p–n-junction regime corresponding to the minimum DOS

$$\begin{cases} \exp\left(\dfrac{-4\sqrt{2qm_e}}{3\hbar|E_{\text{TiO}_x}|}\left((U_{e0})^{\frac{3}{2}} - (U_{e1})^{\frac{3}{2}}\right)\right), & q|\Delta_{\text{TiO}_x}| - \chi_e < E_1 < 0 \\ \exp\left(\dfrac{-4\sqrt{2qm_e}}{3\hbar|E_{\text{TiO}_x}|}(U_{e0})^{\frac{3}{2}}\right), & -\chi_e < qE_1 < q|\Delta_{\text{TiO}_x}| - \chi_e \\ \exp\left(\dfrac{-4\sqrt{2qm_h}}{3\hbar|E_{\text{TiO}_x}|}\left((U_{h0})^{\frac{3}{2}} - (U_{h1})^{\frac{3}{2}}\right)\right), & 0 < qE_1 < \chi_h - q|\Delta_{\text{TiO}_x}| \\ \exp\left(\dfrac{-4\sqrt{2qm_h}}{3\hbar|E_{\text{TiO}_x}|}(U_{h0})^{\frac{3}{2}}\right), & \chi_h - q|\Delta_{\text{TiO}_x}| < qE_1 < \chi_h \\ 1, & qE_1 < -\chi_e \quad \text{or} \quad qE_1 > \chi_h \end{cases} \tag{10}$$

Authorized licensed use limited to: Univ Catholique de Louvain/UCL. Downloaded on February 22,2021 at 15:48:31 UTC from IEEE Xplore. Restrictions apply.

TABLE I
PARAMETERS FOR CONTACT RESISTANCE CALCULATION

Symbol	Definition	Value
t_m	Broadening energy of the grpahene under the metal	0.2 eV, 0.3 eV, 0.4 eV
λ	Length fo the potential step	0 nm, 2 nm, 4 nm
T_{TiO_x}	Thickness of the oxidized Ti	0.5 nm, 0.7 nm
T_{PMMA}	Thickness of the PMMA residues	0.5 nm, 0.7 nm
χ_{TiO_x}	Electron affinity of the oxidized Ti	3.9 eV, 4.0 eV, 4.1 eV [24] [25]
χ_{PMMA}	Electron affinity of the PMMA residues	3.9 eV, 4.0 eV [26], 4.1 eV
ε_{TiO_x}	Relative permittivity of the oxidized Ti	6.9
ε_{PMMA}	Relative permittivity of the PMMA residues	3 [27]
m_e	Electron effective mass in oxidized Ti or PMMA residues	$0.5m_0$, $1.0m_0$, $2m_0$
m_h	Hole effective mass in oxidized Ti or PMMA residues	$0.5m_0$, $1.0m_0$, $2m_0$

m_0 is the free electron mass

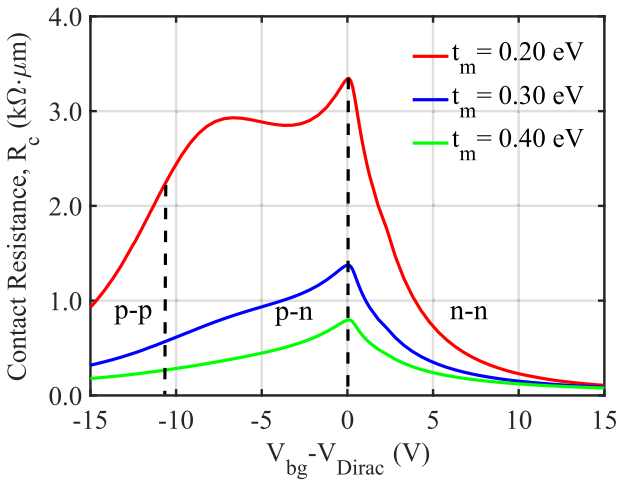


Fig. 4. Calculated contact resistance (R_c) as a function of gate bias for different values of t_m. Fixed parameters used in calculation: $\lambda = 1$ nm, $t_g = 0.2$ eV, $T_{TiO_x} = 0.7$ nm.

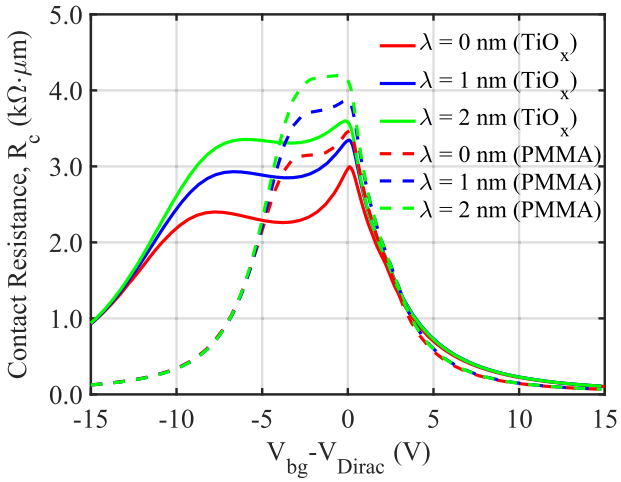


Fig. 5. Calculated contact resistance (R_c) with oxidized Ti or PMMA residues as a function of gate bias for different lengths of the potential step (λ). Fixed parameters used in calculation: $t_m = 0.2$ eV, $t_g = 0.2$ eV, $T_{TiO_x} = 0.7$ nm. $\lambda = 0$ indicates $T_{gg} = 1$.

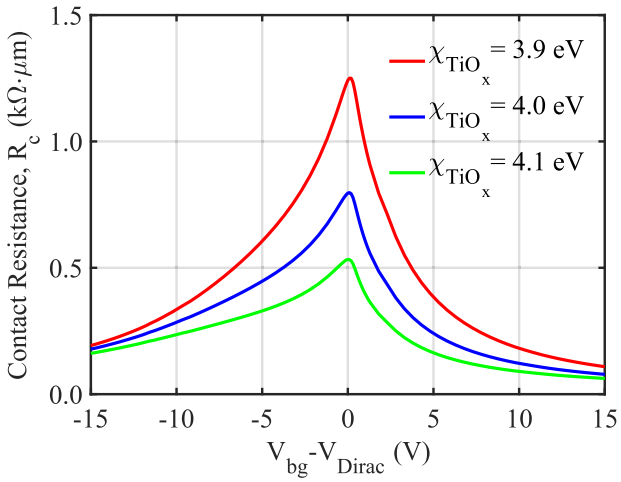


Fig. 6. Calculated contact resistance (R_c) with as a function of gate bias for different electron affinity of the oxidized Ti. Fixed parameters in calculation: $\lambda = 1$ nm, $t_m = 0.4$ eV, $t_g = 0.2$ eV, $T_{TiO_x} = 0.7$ nm.

of graphene under metal ($\phi_{c,m} = 0$). The accurate position of the second peak is found to be dependent on λ. In addition, when $T_m > 0.3$ eV, the second peak vanishes. The potential step can be very sharp ($\lambda < 10$ nm) [28] due to the thin thickness of the silicon oxide we used in this work. The contact resistance increases with the increase of λ in the p–n-junction regime. In the n–n and p–p regions, the contact resistance is independent of λ due to Klein tunneling [29]. Moreover, the contact resistance increases extensively with a slight decrease of t_m according to Fig. 4. Figs. 6 and 7 show the calculated contact resistance as a function of gate bias for different values of electron affinity and effective mass. It is clear that the contact resistance is inversely proportional to both electron affinity and effective mass. A similar result could be obtained for polymethyl methacrylate (PMMA) residues as the interfacial layer.

IV. MODEL ASSESSMENT

In order to validate our model, GFETs has been fabricated. The monolayer graphene was grown on copper foil by Chemical Vapor Deposition [30], the copper foil has been clean by diluted hydrochloric acid solution and deionized (DI) water to avoid any impurities before the graphene synthesis. After the graphene growth, 200-nm-thick PMMA was spin-coated onto the graphene/copper stack followed by 12 h drying in the ambient condition. The copper was etched by diluted mixed acid solution (H_2O_2 + HCL) and rinsed in DI water five times. The PMMA/graphene film was transferred onto a highly p-doped silicon substrate ($N_A \approx 2 \times 10^{19}$ cm^{-3}) with 20-nm-thick silicon oxide. The silicon wafer has been cleaned by the Radio Corporation of America (RCA) method in advance and the oxide was grown in the dry oxidation method. The PMMA was removed by immersion in warm acetone for 30 min. After drying in the ambiance for another

Authorized licensed use limited to: Univ Catholique de Louvain/UCL. Downloaded on February 22,2021 at 15:48:31 UTC from IEEE Xplore. Restrictions apply.

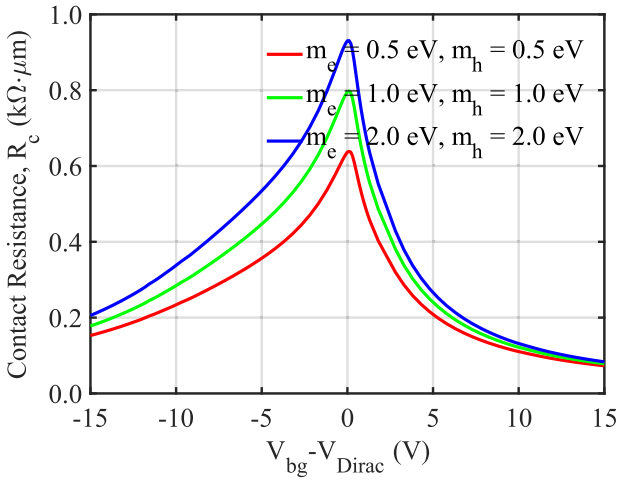


Fig. 7. Calculated contact resistance (R_c) with as a function of gate bias for different effective mass of the oxidized Ti. Parameters used in calculation: $\lambda = 1$ nm, $t_m = 0.4$ eV, $t_g = 0.2$ eV, $T_{TiO_x} = 0.7$ nm.

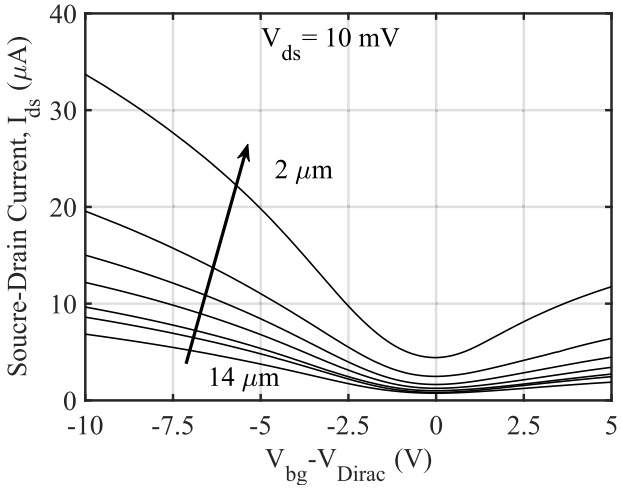


Fig. 8. Averaged source–drain current for all devices corresponding to each channel length as a function of gate bias at $V_{ds} = 10$ mV.

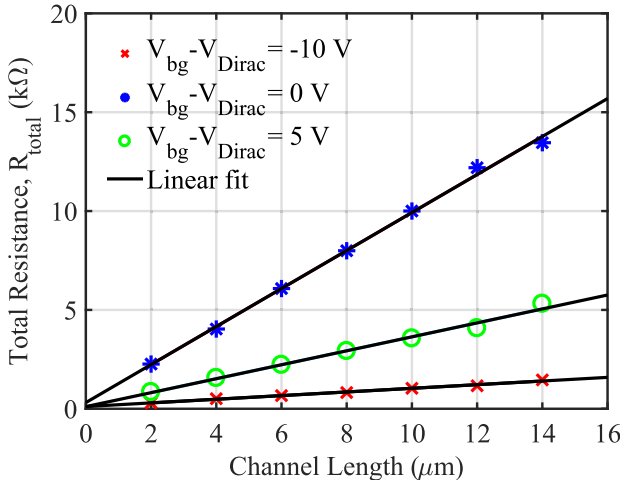


Fig. 9. Deriving contact resistance using TLM at $V_{bg} - V_{\text{Dirac}} = -10$ V (p-doped), 0 V (undoped), 5 V (n-doped).

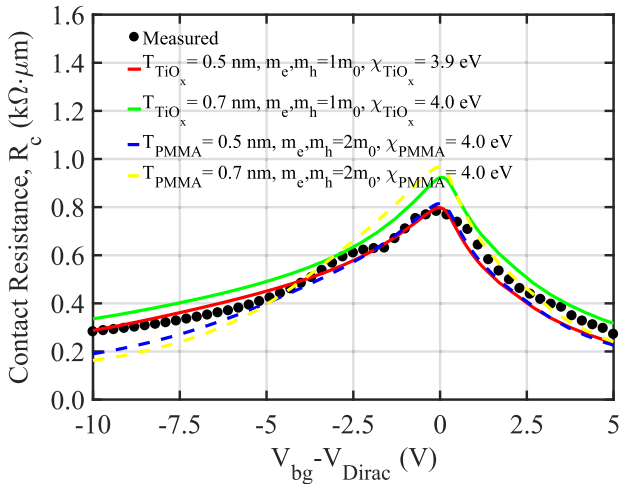


Fig. 10. Measured and Calculated contact resistance (R_c) as a function of gate bias with different parameters of TiO_x and PMMA residues. Fixed parameters in calculation: $\lambda = 1$ nm, $t_m = 0.4$ eV, $t_g = 0.2$ eV.

12 h, the wafer was baked at 150 °C for 15 min to evaporate the trapped water underneath graphene, which improved the adhesion of graphene to the substrate. The graphene channel was patterned by ebeam lithography. The channel width W is 5 μm and the length varies from 2 to 14 μm, in steps of 2 μm. After graphene channel patterning, Ti/Au (5/95 nm) was deposited by e-beam evaporation with a chamber base pressure of 4×10^{-7} mbar and a deposition rate of 0.1 nm/s. No annealing was performed for our devices. 5 nm of Ti is thick enough to be considered as Ti-contact with graphene [4]. The thick Au was deposited to reduce the series resistance of the electrode and avoid further oxidation of Ti in the ambiance.

Measurements were performed in the vacuum at room temperature with $V_{ds} = 10$ mV. The back gate voltage was swept from -9 to 9 V to avoid the breakdown of the thin silicon oxide. More than five arrays of GFETs were measured, Dirac voltages ($\phi_{c,g} = 0$) locate around 3 V $\pm$ 0.5 V, which indicates the p-type doping of the graphene channel possibly due to the H_2O, O_2 or metallic residues adsorbed on the graphene after the transfer. We used the averaged values of all the devices corresponding to each channel length to extract the contact resistance by transmission line method.

The averaged source–drain current I_{ds} of each channel length as a function of gate bias is presented in Fig. 8. The minimum carrier density (n_0) of graphene channel was extracted using the quasi-static model proposed by Haddad *et al.* [20] and has been approximated to be 1×10^{12}–1.5×10^{12} cm^{-3}. Three typical fitting results are presented in Fig. 9, the symbols denote the measured source–drain resistance R_{total} and lines are the fitting curves. The fitted contact resistance R_c is 282.17 $\Omega \cdot\mu$m, 783.95 $\Omega \cdot\mu$m and 271.45 $\Omega \cdot\mu$m at gate biases of $V_{bg} - V_{\text{Dirac}} = -10$, 0, 5 V, respectively, with fitting confidence of 95%. Fig. 10 shows the extracted and calculated contact resistance with different properties of the oxidized Ti layer and the PMMA residues. The main peak at Dirac voltage has been obviously observed, while the second peak corresponding to the Dirac point of the graphene underneath the metal

Authorized licensed use limited to: Univ Catholique de Louvain/UCL. Downloaded on February 22,2021 at 15:48:31 UTC from IEEE Xplore. Restrictions apply.

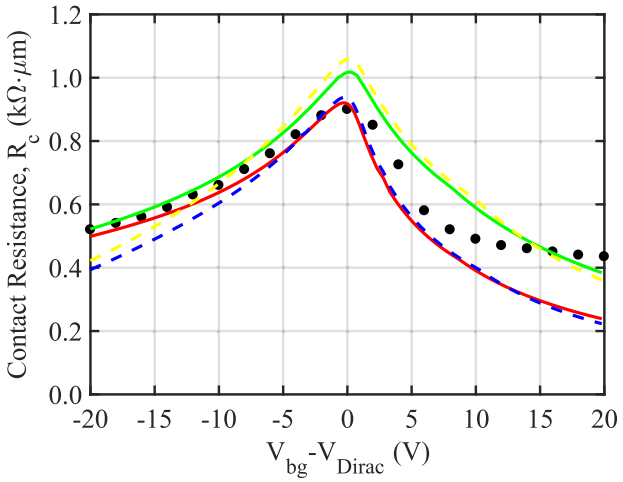


Fig. 11. Reported and calculated contact resistance (R_c) as a function of gate bias with different properties of the interfacial layer. The parameters corresponding to each curve are shown below. Red curve: $T_{TiO_x} = 0.6$ nm, t_g= 0.167eV, $\lambda = 2$ nm, $m_e = m_h = 1m_0$, $\chi_{TiO_x} = 4.0$ eV. Green Curve: $T_{TiO_x} = 0.5$ nm, $t_g = 0.2$ eV, $\lambda = 1$ nm, $m_e = 0.5m_0$, $m_h = 2m_0$, $\chi_{TiO_x} = 3.9$ eV. Blue curve: $T_{PMMA} = 0.6$ nm, $t_g = 0.167$ eV, $\lambda = 2$ nm, $m_e = 0.5m_0$, $m_h = 2m_0$, $\chi_{TiO_x} = 3.9$ eV. Yellow curve: $T_{PMMA} = 0.5$ nm, $t_g = 0.2$ eV, $\lambda = 2$ nm, $m_e = m_h = 1m_0$, $\chi_{TiO_x} = 3.9$ eV. Fixed parameters in calculation: $t_m = 0.4$ eV, $t_g = 0.167$ eV.

vanishes, indicating a large value of t_m (> 0.3 eV). The weak peak at around $V_{bg} - V_{\text{Dirac}} = -2.5$ V may be due to the fitting error from the contact resistance extraction by TLM method. For both TiO_x and PMMA residues, we have obtained well-fitted calculation results with proper properties of the interfacial layer. We also benchmarked our model against the experimental data reported by Xia *et al.* [10] which is shown in Fig. 11, 90-nm-thick silicon oxide was used in their experiment. Our model also fits the reported data well in the p–p and p–n regimes.

V. Conclusion

In conclusion, the contact resistance of Ti–graphene contact has been investigated theoretically and experimentally. A low value of 271.45 $\Omega \cdot \mu$m of contact resistance at room temperature was obtained. Based on quantum tunneling theory, we have presented a physical model of the contact resistance considering an interfacial layer including oxidized Ti and PMMA residues at the Ti–graphene interface. The transmission possibility through Ti-IL–graphene stack has been modeled and applied into the simulation of the graphene contact resistance. This study indicates the contact resistance is highly dependent on the properties of the interfacial layer. Our model is able to explain and evaluate the graphene contact resistance in realistic processing conditions.

Acknowledgment

The authors would like to thank the Wallonia Infrastructure for Nano Fabrication (WINFAB) and the Wallonia Electronics and Communications Measurements (WELCOME) platforms for access to the experimental facilities.

References

[1] K. S. Novoselov, "Electric field effect in atomically thin carbon films," *Science*, vol. 306, no. 5696, pp. 666–669, Oct. 2004, doi: 10.1126/science.1102896.

[2] A. H. Castro Neto, F. Guinea, N. M. R. Peres, K. S. Novoselov, and A. K. Geim, "The electronic properties of graphene," *Rev. Mod. Phys.*, vol. 81, no. 1, pp. 109–162, Jan. 2009, doi: 10.1103/RevModPhys.81.109.

[3] G. Giovannetti, P. A. Khomyakov, G. Brocks, V. M. Karpan, J. van den Brink, and P. J. Kelly, "Doping graphene with metal contacts," *Phys. Rev. Lett.*, vol. 101, no. 2, Jul. 2008, Art. no. 026803, doi: 10.1103/PhysRevLett.101.026803.

[4] P. A. Khomyakov, G. Giovannetti, P. C. Rusu, G. Brocks, J. van den Brink, and P. J. Kelly, "First-principles study of the interaction and charge transfer between graphene and metals," *Phys. Rev. B, Condens. Matter*, vol. 79, no. 19, May 2009, Art. no. 195425, doi: 10.1103/PhysRevB.79.195425.

[5] O. Balci and C. Kocabas, "Rapid thermal annealing of graphene-metal contact," *Appl. Phys. Lett.*, vol. 101, no. 24, Dec. 2012, Art. no. 243105, doi: 10.1063/1.4769817.

[6] K. Nagashio, T. Nishimura, K. Kita, and A. Toriumi, "Contact resistivity and current flow path at metal/graphene contact," *Appl. Phys. Lett.*, vol. 97, no. 14, Oct. 2010, Art. no. 143514, doi: 10.1063/1.3491804.

[7] M. Zhu, J. Wu, Z. Du, S. Tsang, and E. H. T. Teo, "Gate voltage and temperature dependent ti-graphene junction resistance toward straightforward p-n junction formation," *J. Appl. Phys.*, vol. 124, no. 21, Dec. 2018, Art. no. 215302, doi: 10.1063/1.5052589.

[8] F. Driussi, S. Venica, A. Gahoi, S. Kataria, M. C. Lemme, and P. Palestri, "Dependability assessment of transfer length method to extract the metal–graphene contact resistance," *IEEE Trans. Semicond. Manuf.*, vol. 33, no. 2, pp. 210–215, May 2020.

[9] S. Venica, F. Driussi, A. Gahoi, P. Palestri, M. C. Lemme, and L. Selmi, "On the adequacy of the transmission line model to describe the graphene–metal contact resistance," *IEEE Trans. Electron Devices*, vol. 65, no. 4, pp. 1589–1596, Apr. 2018.

[10] F. Xia, V. Perebeinos, Y.-M. Lin, Y. Wu, and P. Avouris, "The origins and limits of metal–graphene junction resistance," *Nature Nanotechnol.*, vol. 6, no. 3, pp. 179–184, Mar. 2011, doi: 10.1038/nnano.2011.6.

[11] X. Ji, J. Zhang, Y. Wang, H. Qian, and Z. Yu, "A theoretical model for metal–graphene contact resistance using a DFT–NEGF method," *Phys. Chem. Chem. Phys.*, vol. 15, pp. 17883–17886, 2013, doi: 10.1039/C3CP52589A.

[12] F. A. Chaves, D. Jiménez, A. A. Sagade, W. Kim, J. Riikonen, H. Lipsanen, and D. Neumaier, "A physics-based model of gate-tunable metal–graphene contact resistance benchmarked against experimental data," *2D Mater.*, vol. 2, no. 2, May 2015, Art. no. 025006, doi: 10.1088/2053-1583/2/2/025006.

[13] W. Li *et al.*, "Ultraviolet/ozone treatment to reduce metal-graphene contact resistance," *Appl. Phys. Lett.*, vol. 102, no. 18, May 2013, Art. no. 183110.

[14] W. S. Leong, C. T. Nai, and J. T. L. Thong, "What does annealing do to metal–graphene contacts?" *Nano Lett.*, vol. 14, no. 7, pp. 3840–3847, 2014, doi: 10.1021/nl500999r.

[15] J. A. Robinson *et al.*, "Contacting graphene," *Appl. Phys. Lett.*, vol. 98, no. 5, Jan. 2011, Art. no. 053103, doi: 10.1063/1.3549183.

[16] C. M. Corbet, C. McClellan, K. Kim, S. Sonde, E. Tutuc, and S. K. Banerjee, "Oxidized titanium as a gate dielectric for graphene field effect transistors and its tunneling mechanisms," *ACS Nano*, vol. 8, no. 10, pp. 10480–10485, Oct. 2014, doi: 10.1021/nn5038509.

[17] K. M. Freedy, A. Giri, B. M. Foley, M. R. Barone, P. E. Hopkins, and S. McDonnell, "Titanium contacts to graphene: Process-induced variability in electronic and thermal transport," *Nanotechnology*, vol. 29, no. 14, Feb. 2018, Art. no. 145201, doi: 10.1088/1361-6528/aaaacd.

[18] M. Politou *et al.*, "Transition metal contacts to graphene," *Appl. Phys. Lett.*, vol. 107, no. 15, Oct. 2015, Art. no. 153104, doi: 10.1063/1.4933192.

[19] J. G. Champlain, "A first principles theoretical examination of graphene-based field effect transistors," *J. Appl. Phys.*, vol. 109, no. 8, Apr. 2011, Art. no. 084515, doi: 10.1063/1.3573517.

[20] P.-A. Haddad, D. Flandre, and J.-P. Raskin, "A quasi-static model of silicon substrate effects in graphene field effect transistors," *IEEE Electron Device Lett.*, vol. 38, no. 7, pp. 987–990, Jul. 2017, doi: 10.1109/LED.2017.2706362.

Authorized licensed use limited to: Univ Catholique de Louvain/UCL. Downloaded on February 22,2021 at 15:48:31 UTC from IEEE Xplore. Restrictions apply.

[21] S. Sze and K. K. Ng, *Physics of Semiconductor Devices: Sze/Physics*. Hoboken, NJ, USA: Wiley, Oct. 2006, doi: 10.1002/0470068329.

[22] S. Datta, *Electronic Transport in Mesoscopic Systems* (Cambridge Studies in Semiconductor Physics and Microelectronic Engineering). Cambridge, U.K.: Cambridge Univ. Press, 1995, doi: 10.1017/CBO9780511805776.

[23] J. Cayssol, B. Huard, and D. Goldhaber-Gordon, "Contact resistance and shot noise in graphene transistors," *Phys. Rev. B*, vol. 79, no. 7, Feb. 2009, Art. no. 075428, doi: 10.1103/PhysRevB.79.075428.

[24] S. Hu, M. R. Shaner, J. A. Beardslee, M. Lichterman, B. S. Brunschwig, and N. S. Lewis, "Amorphous TiO_2 coatings stabilize Si, GaAs, and GaP photoanodes for efficient water oxidation," *Science*, vol. 344, no. 6187, pp. 1005–1009, May 2014, doi: 10.1126/science.1251428.

[25] J. Robertson, "Band offsets of wide-band-gap oxides and implications for future electronic devices," *J. Vac. Sci. Technol. B, Microelectron.*, vol. 18, no. 3, pp. 1785–1791, 2000, doi: 10.1116/1.591472.

[26] S. Peng, Z. Jin, D. Zhang, J. Shi, Y. Zhang, and G. Yu, "Evidence of electric field-tunable tunneling probability in graphene and metal contact," *Nanoscale*, vol. 9, no. 27, pp. 9520–9528, 2017, doi: 10.1039/C7NR02502E.

[27] A. Sanne, H. C. P. Movva, S. Kang, C. McClellan, C. M. Corbet, and S. K. Banerjee, "Poly(methyl methacrylate) as a self-assembled gate dielectric for graphene field-effect transistors," *Appl. Phys. Lett.*, vol. 104, no. 8, Feb. 2014, Art. no. 083106, doi: 10.1063/1.4866338.

[28] F. A. Chaves, D. Jiménez, J. E. Santos, P. Bøggild, and J. M. Caridad, "Electrostatics of metal–graphene interfaces: Sharp p–n junctions for electron-optical applications," *Nanoscale*, vol. 11, pp. 10273–10281, 2019, doi: 10.1039/C9NR02029B.

[29] M. I. Katsnelson, K. S. Novoselov, and A. K. Geim, "Chiral tunnelling and the klein paradox in graphene," *Nature Phys.*, vol. 2, no. 9, pp. 620–625, Sep. 2006, doi: 10.1038/nphys384.

[30] B. Huet and J.-P. Raskin, "Role of cu foil *in-situ* annealing in controlling the size and thickness of CVD graphene domains," *Carbon*, vol. 129, pp. 270–280, Apr. 2018, doi: 10.1016/j.carbon.2017.12.043.

Authorized licensed use limited to: Univ Catholique de Louvain/UCL. Downloaded on February 22,2021 at 15:48:31 UTC from IEEE Xplore. Restrictions apply.